Journal of Biomechanics 86 (2019) 71–78

Contents lists available at ScienceDirect

Journal of Biomechanics

journal homepage: www.elsevier.com/locate/jbiomech
www.JBiomech.com

Reliability and robustness of muscle architecture measurements obtained using diffusion tensor imaging with anatomically constrained tractography

Bart Bolsterlee *, Arkiev D'Souza, Robert D. Herbert

Neuroscience Research Australia, Sydney, NSW, Australia
University of New South Wales, Sydney, NSW, Australia

ARTICLE INFO

Article history:
Accepted 22 January 2019

Keywords:
Muscle architecture
Diffusion tensor imaging
Magnetic resonance imaging
Three-dimensional
Fascicle length
Pennation

ABSTRACT

For detailed analyses of muscle adaptation mechanisms during growth, ageing or disease, reliable measurements of muscle architecture are required. Diffusion tensor imaging (DTI) and DTI tractography have been used to reconstruct the architecture of human muscles *in vivo*. However, muscle architecture measurements reconstructed with conventional DTI techniques are often anatomically implausible because the reconstructed fascicles do not terminate on aponeuroses, as real muscle fascicles are known to do. In this study, we tested the reliability of an anatomically constrained DTI-based method for measuring three-dimensional muscle architecture. Anatomical magnetic resonance images and diffusion tensor images were obtained from the left legs of eight healthy participants on two occasions one week apart. Muscle volumes, fascicle lengths, pennation angles and fascicle curvatures were measured in the medial and lateral gastrocnemius, soleus and the tibialis anterior muscles. Averaged across muscles, the intraclass correlation coefficient was 0.99 for muscle volume, 0.81 for fascicle length, 0.73 for pennation angle and 0.76 for fascicle curvature. Measurements of muscle architecture obtained using conventional DTI tractography were highly sensitive to variations in the stopping criteria for DTI tractography. The application of anatomical constraints reduced this sensitivity significantly. This study demonstrates that anatomically constrained DTI tractography can provide reliable and robust three-dimensional measurements of whole-muscle architecture. The algorithms used to constrain tractography have been made publicly available.

1. Introduction

In vivo measurements of the physical arrangement of muscle fibres ("muscle architecture") are required to study organ-level mechanisms of muscle force production and adaptation. To date, most studies of human muscle architecture have obtained two-dimensional measurements of muscle architecture using ultrasound imaging, but two-dimensional imaging is potentially problematic because most human muscles have complex architectures that can only accurately be described in three dimensions (3D) (Agur et al., 2003; Bolsterlee et al., 2017; Lee et al., 2015). The functional relevance of the 3D architecture of muscles is becoming increasingly understood (Azizi et al., 2008; Blemker et al., 2005; Böl et al., 2013; Raiteri et al., 2018; Ross et al., 2018), but only limited data are available on three-dimensional muscle architecture in human muscles, and how three-dimensional muscle architecture changes with, for example, training, age or disease.

Though initially developed and applied to study the neuroanatomy of the brain (Basser et al., 1994; Basser and Pierpaoli, 1996), diffusion tensor imaging (DTI; a magnetic resonance imaging technique) is now used increasingly to reconstruct the 3D architecture of human skeletal muscles (Damon et al., 2017; Oudeman et al., 2015). DTI-based measurements of muscle architecture rely on the principle that the diffusion rate of water molecules is higher in the longitudinal direction of muscle fibres than in the fibre's transverse plane. DTI measures, for each voxel of the scan, the direction in which diffusion rates are highest (the primary diffusion direction), providing a local measure of muscle fibre orientation. The three-dimensional architecture of muscles can be reconstructed by generating curves that propagate along the primary diffusion

* Corresponding author at: Neuroscience Research Australia, Margarete Ainsworth Building, 139 Barker Street, 2031 Randwick, New South Wales, Australia.
E-mail address: b.bolsterlee@neura.edu.au (B. Bolsterlee).

https://doi.org/10.1016/j.jbiomech.2019.01.043
0021-9290/

direction throughout the muscle (Bolsterlee et al., 2017; Froeling et al., 2012). This procedure is called DTI tractography and the resulting curves are called fibre tracts. Although fibre tracts cannot be interpreted directly as muscle fascicles (because the number of tracts generated within a muscle is arbitrary, and they are infinitely thin), tracts follow the direction of muscle fibres and can thus be used to obtain three-dimensional, quantitative measures of muscle architecture such as fascicle lengths, pennation angles and fibre curvatures (Bolsterlee et al., 2017).

A problem with conventional DTI tractography algorithms is that the fibre tracts do not necessarily terminate on tendons or aponeuroses, as muscle fascicles are known to do. Instead, with conventional tractography, fibre tracts terminate when stopping criteria are satisfied. Typically, stopping criteria are satisfied when the maximum angle between subsequent tract segments (the turning angle) exceeds a certain threshold, or when the fractional anisotropy (FA) falls outside a certain range (Froeling et al., 2013; Heemskerk et al., 2009). The turning angle criterion is designed to terminate propagation of fibre tracts when they reach the boundary of the muscle where tract orientation often changes sharply. The FA criterion serves to exclude fibre tracts that penetrate tissues other than muscle, such as skin and adipose tissue, on the basis of differences in the diffusion properties of these tissues. There have been no published reports of investigations of specific stopping criteria on measurements of muscle architecture, and it is possible that optimal stopping criteria may vary between scans and muscles. In practice, the fibre tracts generated with conventional tractography methods frequently terminate intramuscularly or extend into adjacent muscles. Measurements of muscle architecture based on implausible representations of muscle fascicles are likely to be inaccurate.

We have recently developed a method in which anatomical constraints are applied to DTI tractography so that fibre tracts are made to terminate on tendinous structures (Bolsterlee et al., 2017; Bolsterlee et al., 2018). This method, which operates in three dimensions, is conceptually similar to the two-dimensional extrapolation techniques commonly used to measure muscle architecture from ultrasound images, where the visible parts of fascicles are extrapolated to aponeuroses (Cronin and Lichtwark, 2013; Fukunaga et al., 1997; Herbert et al., 2015). In our approach, polynomial curves are fitted to the fibre tracts, as was done previously by Damon et al. (2012), and the polynomials are then linearly extrapolated to terminate on tendons or aponeuroses.

In previous studies we have demonstrated that the application of anatomical constraints leads to realistic reconstructions of the medial gastrocnemius and soleus muscles (Bolsterlee et al., 2017; Bolsterlee et al., 2018). In the present study, we generalize the method to muscles with bipennate architectures and intramuscular aponeuroses (e.g. tibialis anterior) and determine the test-retest reliability of the architecture measurements. We then demonstrate that the application of anatomical constraints reduces the sensitivity of muscle architecture measurements to the stopping criteria used for DTI tractography. To facilitate use of these techniques, Matlab algorithms to apply anatomical constraints to DTI tractography are made available for public use.

2. Methods

This study was conducted on eight young adults with no known musculoskeletal pathology or injury in the lower limb (Table 1). All procedures conformed to the 2008 Declaration of Helsinki and were approved by University of New South Wales' Human Research Ethics Committee (approval HC17106). Informed, written, voluntary consent was obtained prior to participation.

Table 1
Characteristics of participants and joint position during measurements.

Characteristic	Value
Age (years)	31 ± 6
Gender (M:F)	4:4
Height (cm)	170 ± 8
Weight (kg)	72 ± 16
Shank length (cm)*	39 ± 3
Knee angle (°)§	18 ± 7
Ankle angle (°)†	87 ± 3

* Distance from the lateral femoral condyle to the middle of the lateral malleolus.
† Angle between the tibia and the sole of the foot, where 90° is a neutral ankle joint orientation and values below and above 90° indicate plantarflexion and dorsiflexion, respectively.
§ Angle between the tibia and the thigh, where 0° is full knee extension.

2.1. Image acquisition

T1-weighted, mDixon and DTI scans were obtained of the left lower leg of all participants on two days with seven days between scans. Participants were placed in a 3-T MRI scanner (Achieva TX, Philips Medical Systems, Best, The Netherlands) in a supine position. The left foot was placed in an MRI-compatible foot plate which made an angle of 70° with the horizontal plane. The knee was positioned in slight flexion (on average 18°; Table 1) by putting a foam wedge under the knee so that the calf did not touch the MRI table and the calf muscles were not compressed by the weight of the leg. A cardiac coil with 32 elements for receive was placed around the lower leg.

The MRI protocol consisted of three sequences: T1-weighted and mDixon imaging for anatomical reference, and diffusion tensor imaging for fibre architecture reconstructions. The following imaging parameters were used. *mDixon:* 2-point 3D multi-echo mDixon fast field echo (FFE), field of view (FOV) = 180 × 180 mm, acquisition matrix = 180 × 180 (reconstructed matrix = 192 × 192); slice = 2 mm (1 mm over-contiguous), 160 slices, TR/TE1/TE2 = 6.0/3.5/4.6 msec, number of signal averages (NSA) = 2, scan time = 346 s. *T1-weighted:* 2D turbo spin echo (TSE), FOV = 180 × 180 mm, acquisition matrix 288 × 210 (reconstructed matrix = 864 × 864), slice = 4 mm, 80 slices, TR/TE = 638/5.7 msec, flip angle = 80°, NSA = 1, scan time = 258 s; *DTI:* spin echo echo-planar imaging (SE-EPI), FOV = 180 × 180 mm, acquisition matrix 92 × 90 (reconstructed to 112 × 112), slice = 5 mm, 50 slices, TR/TE = 9501/64 msec, diffusion gradient timing Δ/δ = 32/8 msec, EPI factor = 45, NSA = 4, 16 gradient directions on a hemisphere, b = 500 s/mm^2 (reference image with b = 0 s/mm^2), scan time = 637 s. Fat was suppressed using spectral attenuated inversion recovery (SPAIR) and Dixon olefinic fat suppression using a 180 Hz pre-pulse (Burakiewicz et al., 2018). To correct for local inhomogeneities in the magnetic field, the DTI scan was preceded by a B_0-calibration using the following settings: 3D FFE, FOV = 180 × 180 mm (reconstructed matrix = 96 × 96), slice = 5 mm, 50 slices, TR/TE/ΔTE = 30/4.6/2.3 msec, NSA = 2.

2.2. DTI post-processing

The DTI data were corrected for small eddy current-induced distortions using algorithms built into FSL (Andersson and Sotiropoulos, 2016) and then filtered using a local principal component analysis filter (Manjon et al., 2013). Although all imaging was performed without repositioning the participant, small misalignments between the mDixon, DTI and T1 scans were still

present. To correct for these misalignments, T1 and DTI scans were aligned with the mDixon scan using Elastix registration software (v4.8; Klein et al., 2010). The T1 scan was aligned with the corresponding mDixon scan using a rigid registration and the DTI scan was aligned with the corresponding mDixon scan using a rigid registration, followed by an affine registration. The result of registration was inspected by overlaying the DTI and T1 scan on the mDixon scan in ITK-SNAP and visually confirming that features that were visible on all scans (skin/bone/muscle boundaries) were well aligned (v3.6.0; Yushkevich et al., 2006).

From the eddy-current corrected, filtered and registered DTI data, the diffusion tensor was reconstructed using DSI Studio (Yeh et al., 2013), after which the primary eigenvector direction and diffusion properties (primary, secondary and tertiary eigenvalues, mean diffusivity and fractional anisotropy [FA]) were extracted for all voxels.

2.3. Muscle and aponeurosis segmentation

Using ITK-snap (v3.6.0; Yushkevich et al., 2006), the medial gastrocnemius (MG), lateral gastrocnemius (LG), soleus and tibialis anterior muscles (TA) were manually segmented on the out-of-phase image of the mDixon scan. The soleus was subdivided in four compartments (as done previously; Bolsterlee et al., 2018): lateral-anterior (SLA), medial-anterior (SMA), lateral-posterior (SLP), medial-posterior (SMP). Only scans obtained on the first day were manually segmented. To segment the scans obtained on the second day (one week later), Elastix was used to register the water-image of the mDixon scans obtained on the first and second days using a combination of rigid and non-rigid registration (b-spline transformation with grid size 20 × 20 × 20 mm) and then applying the transformation to the boundaries obtained by manual segmentation on the first day. The predicted segmentations were visually inspected using ITK-snap and, where necessary, manually corrected.

The internal aponeurosis of the tibialis anterior muscle was segmented on the T1-weighted anatomical scan (using 3D slicer v4.7.0; Fedorov et al., 2012), because this scan gave better contrast between the aponeurosis and surrounding muscle tissue than the mDixon scan.

Using the segmentations, 3D triangulated surface meshes of the muscle boundaries and tibialis anterior aponeurosis were created using the Matlab-based iso2mesh toolbox (Fang and Boas, 2009) (Matlab R2017a, The MathWorks, Inc., Natick, United States).

2.4. DTI tractography

DTI tractography was performed using a deterministic tractography algorithm built into DSI Studio (Yeh et al., 2013). Fibre tracts were propagated bi-directionally from seed points placed on a 3 × 3 × 3 mm grid within each muscle. The following default settings were used for fibre tractography in all muscles: $0.1 \leq FA \leq 0.5$, step size = 1 mm and maximum turning angle = 10°. Only fibre tracts that had lengths larger than 20 mm and smaller than 200 mm were included (Table 2).

The curves generated by DTI tractography will be referred to as fibre tracts, and their lengths as tract lengths. The endpoints of fibre tracts are determined exclusively by the tractography stopping criteria. The procedures that will be described next use fibre tracts to generate what we refer to here as 'muscle fascicles'. The endpoints of muscle fascicles are constrained to terminate on tendons or aponeuroses (Bolsterlee et al., 2017; Bolsterlee et al., 2018).

2.5. Muscle architecture measurements

Each fibre tract was fitted with a three-dimensional third-order polynomial curve. The slope at either endpoint of the curve was calculated, and the curve was then extended at the endpoints by linearly projecting the curve along the endpoint's slope onto the muscle surface. The polynomial curve including the extensions is referred to as a fascicle. Only fascicles whose extensions were less than 30% of the total fascicle length were included in further analyses. For the tibialis anterior, only fascicles that had one attachment on the internal aponeurosis and one on the muscle boundary were included. Fig. 1 shows examples of fascicle reconstructions.

Fascicle length was calculated as the length of the polynomial curve including the extensions. The pennation angle at each of the fascicle's attachments to an aponeurosis was calculated as 90° minus the mean angle between a vector parallel to the endpoint's slope and the normal vectors of all triangles of the surface model within a radius of 1.5 mm around the endpoint. Pennation was the mean of the angles that the fascicle made with the deep and superficial aponeuroses. The curvature of a fascicle (expressed as 1/radius of curvature [m^{-1}]) was calculated using the Frenet-Serret formula as the mean curvature of 100 equidistant points along the polynomial curve of that fascicle.

All algorithms to reconstruct fascicles and calculate architectural parameters were developed in Matlab R2017a and have been made available on GitHub (github.com/bartbols/muscle_architecture_DTI).

2.6. Reliability

The test-retest reliability of muscle architecture measurements was determined for each muscle by comparing between days the median measurements of fascicle length, pennation angle and cur-

Table 2
Quality of fibre tracking and fascicle reconstructions. For each muscle, the mean ± standard deviation from all participants and both days is presented (n = 16). The last row presents the mean ± standard deviation of the muscles' means.

Muscle	Number of seeds[a]	Number of fibres (% of number of seeds)[b]	Number of fascicles (% of number of fibres)[c]	Number of fascicles	Extension (mm)	Extension (% of fascicle length)
MG	7059 ± 1954	65 ± 13	56 ± 16	2450 ± 864	6 ± 3	10 ± 3
LG	3751 ± 1345	75 ± 9	58 ± 12	1597 ± 622	5 ± 2	8 ± 4
SMP	5564 ± 1931	57 ± 18	64 ± 15	2050 ± 1075	5 ± 2	11 ± 3
SMA	953 ± 477	52 ± 28	46 ± 23	241 ± 224	7 ± 2	15 ± 5
SLP	5921 ± 2598	60 ± 14	51 ± 16	1602 ± 503	9 ± 2	17 ± 4
SLA	1370 ± 792	49 ± 25	60 ± 24	447 ± 454	4 ± 2	12 ± 5
TA	4579 ± 1372	64 ± 14	46 ± 9	1286 ± 382	3 ± 1	6 ± 2
Average	4171 ± 2305	60 ± 9	54 ± 7	1382 ± 803	5 ± 2	11 ± 4

MG = medial gastrocnemius; LG = lateral gastrocnemius; SMP = soleus medial-posterior; SMA = soleus medial-anterior; SLP = soleus lateral-posterior; SLA = soleus lateral-anterior; TA = tibialis anterior

[a] The number of locations in the muscle from which fibre tracking was attempted. In all muscles, seeds were placed on a 3 × 3 × 3 mm grid, so the number of seeds reflects the muscle size.

[b] The fraction of seeds that led to successful fibre tracts, i.e. fibre tracts that were longer than 20 mm and shorter than 200 mm.

[c] The fraction of fibre tracts from which fascicles were successfully reconstructed (i.e. fascicles that were extended by less than 30% to have endpoints on the aponeuroses).

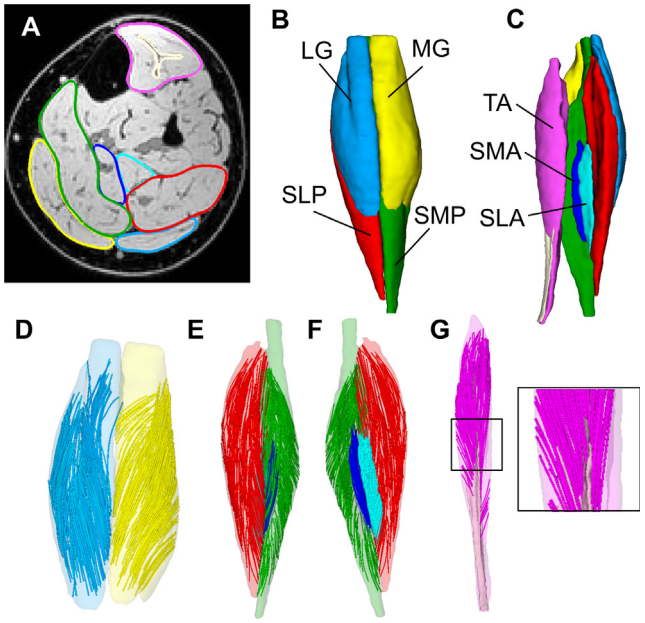

Fig. 1. Overview of methods to measure muscle architecture from anatomical and DTI scans. (A) Transverse slice of the mDixon scan (water image) approximately midway between the ankle and knee joint, showing outlines of the muscles, muscle compartments and the tibialis internal aponeurosis. Posterior view (B) and anterior view (C) of the three-dimensional reconstructions of the muscles. Muscle architecture reconstructions of the MG and LG (D), soleus (E; left posterior view, F; right anterior view) and tibialis anterior (G; inset is a detailed view showing the bipennate architecture of the TA). MG = medial gastrocnemius (yellow), LG = lateral gastrocnemius (light blue), SMP = soleus medial-posterior (dark green), SMA = soleus medial-anterior (dark blue), SLP = soleus lateral-posterior (red), SLA = soleus lateral-anterior (cyan), TA = tibialis anterior (magenta).

vature of all fascicles that were reconstructed in that muscle. Reliability was measured as the absolute-agreement intraclass correlation coefficient (ICC (2,1) (McGraw and Wong, 1996)) and standard error of the mean (SEM).

2.7. Sensitivity analysis

To determine the sensitivity of muscle architecture measurements to DTI tractography parameters, fibre tracking and fascicle reconstructions were repeated for all muscles by altering, one at a time, the turning angle, minimum fractional anisotropy threshold and step size. The maximum turning angle (default: 10°) was changed to 5°, 15° and 20°. The minimum fractional anisotropy threshold (default: 0.1) was changed to 0.05 and 0.15. The step size (default: 1 mm) was changed to 0.5 and 1.5 mm. Median tract lengths (without application of anatomical constraints) and median fascicle lengths (after application of anatomical constraints) were calculated for all muscles and stopping criteria, and their differences with the values obtained using the default stopping criteria were calculated.

The effect of polynomial order on median fascicle length, pennation angle and fascicle curvature was calculated for all muscles by changing the polynomial order to 1 (i.e. straight fascicles), 2 and 4, and then calculating the difference with the default value (order = 3) for all muscles.

3. Results

Fascicles were reconstructed and architectural measurements were obtained successfully for all muscles and participants. The number of seeds from which fibre tracking was attempted ranged from 953 in the smallest muscle (SMA) to 7059 in the largest

Table 3
Muscle architecture measurements on day 1 and day 2 (mean ± standard deviation) and the test-retest reliability of muscle architecture measurements expressed as intraclass correlation coefficients (ICC with 95% confidence intervals in brackets) and standard error of the mean (SEM).

Variable	Muscle	Day 1	Day 2	ICC	SEM
Muscle volume (cm^3)	MG	256.9 (63.5)	245.9 (64.7)	0.98 (0.67 to 1.00)	6.8
	LG	140.0 (51.3)	134.1 (49.1)	0.99 (0.82 to 1.00)	3.4
	SMP	179.7 (64.5)	178.2 (66.0)	0.99 (0.97 to 1.00)	5.2
	SMA	32.0 (16.3)	31.8 (15.9)	1.00 (0.99 to 1.00)	0.5
	SLP	191.7 (84.7)	191.8 (87.6)	1.00 (0.99 to 1.00)	3.6
	SLA	45.8 (26.1)	45.7 (25.5)	1.00 (1.00 to 1.00)	0.5
	TA	146.2 (42.5)	144.5 (43.0)	0.99 (0.96 to 1.00)	4
Fascicle length (mm)	MG	61.0 (18.1)	64.4 (24.6)	0.92 (0.67 to 0.98)	4.1
	LG	67.8 (11.3)	63.8 (10.2)	0.84 (0.32 to 0.97)	3.5
	SMP	42.7 (10.1)	39.5 (7.8)	0.82 (0.34 to 0.96)	3.0
	SMA	46.3 (16.5)	51.0 (14.3)	0.82 (0.38 to 0.96)	5.9
	SLP	53.8 (10.7)	53.6 (10.7)	0.91 (0.60 to 0.98)	3.4
	SLA	39.9 (7.3)	38.0 (7.9)	0.80 (0.33 to 0.95)	3.3
	TA	50.0 (8.0)	44.9 (8.6)	0.58 (−0.05 to 0.89)	4.8
Pennation angle (°)	MG	21.1 (4.9)	20.6 (5.5)	0.95 (0.80 to 0.99)	1.1
	LG	16.5 (2.6)	17.4 (3.3)	0.89 (0.49 to 0.98)	0.6
	SMP	24.6 (4.5)	25.7 (4.3)	0.91 (0.58 to 0.98)	1.2
	SMA	19.0 (4.1)	21.3 (4.7)	0.14 (−0.53 to 0.73)	4.0
	SLP	21.2 (5.2)	22.0 (4.8)	0.93 (0.73 to 0.99)	1.2
	SLA	20.0 (3.9)	22.6 (3.8)	0.60 (−0.05 to 0.90)	2.0
	TA	19.5 (1.9)	21.5 (3.2)	0.52 (−0.10 to 0.88)	1.3
Curvature (1/m)	MG	9.7 (3.0)	9.0 (3.1)	0.95 (0.67 to 0.99)	0.6
	LG	7.4 (1.4)	7.4 (1.7)	0.93 (0.69 to 0.99)	0.4
	SMP	12.7 (3.1)	13.0 (2.7)	0.86 (0.45 to 0.97)	1.1
	SMA	10.9 (4.7)	11.4 (5.1)	0.89 (0.56 to 0.98)	1.7
	SLP	11.0 (2.6)	11.3 (2.8)	0.79 (0.26 to 0.95)	1.3
	SLA	12.3 (4.3)	12.8 (4.8)	0.85 (0.44 to 0.97)	1.8
	TA	8.7 (1.1)	9.1 (0.9)	0.08 (−0.64 to 0.71)	1.0

MG = medial gastrocnemius, LG = lateral gastrocnemius, SMP = soleus medial-posterior, SMA = soleus medial-anterior, SLP = soleus lateral-posterior, SLA = soleus lateral-anterior, TA = tibialis anterior.

muscle (MG; Table 2). On average, 60% of the seeds (range between muscles: 49–65%) led to successful fibre tracts, i.e. tracts for which the stopping criteria were reached at tract lengths larger than 20 mm and smaller than 200 mm. Of the successful fibre tracts, 54% resulted in successful fascicle reconstructions, i.e. fascicles that were extended by less than 30% of their length to have end-points on the aponeuroses. On average, 1382 fascicles were included per muscle; these were extended by, on average, 5 mm (11% of their length; Table 2).

The reliability of measurements of muscle volume was very high (ICCs between 0.98 and 1.00; Table 3 and Fig. 2). With just a few exceptions, most architectural parameters of most muscles had high reliability (ICCs between 0.8 and 1.0). Exceptions were measurements of fascicle length and pennation angle of TA and measurements of pennation angle of SMA.

Fibre tract lengths were sensitive to variations in the maximum turning angle (Fig. 3A). Median tract lengths obtained with a turning angle of 5° were, on average, 18 mm shorter than tract lengths obtained with the default turning angle of 10°. With turning angles of 15° and 20°, tracts were longer than the default tracts by an average of 16 and 30 mm, respectively. In contrast, fascicle lengths (tracts to which anatomical constraints had been applied) were much less sensitive to variations in turning angle: with a turning angle of 5°, fascicles were shorter than the default fascicles by 3 mm, and with turning angles of 15° and 20° they were longer by 2 and 4 mm, respectively (Fig. 3B). The lengths of fibre tracts and fascicles were insensitive to changes in fractional anisotropy threshold and step size (Fig. 3A-B). The distributions of the difference between fascicle lengths and tract lengths are displayed in Fig. 3C.

The polynomial order had a small effect on fascicle length and pennation angle measurements (Fig. 4). Differences in polynomial order did not lead to systematically smaller or larger measurements of fascicle length and pennation angle. The mean absolute difference in fascicle length with measurements obtained with polynomial order 3 (the default) was 2.5 mm, 1.2 mm and 0.8 mm for order 1, 2 and 4, respectively. For pennation angle this was 1.9°, 1.4° and 0.5°. Polynomial order affected fibre curvature significantly, and in a systematic manner. Relative to the default fascicle curvatures obtained with order 3, curvatures obtained with order 1 and 2 were smaller by, on average, 10.5/m and 3.1/m. With polynomial order 4, curvatures were larger by 2.1/m.

4. Discussion

We determined the test-retest reliability and robustness of measurements of muscle architecture using a novel DTI tractography method which constrained fibre tracts to terminate on aponeuroses. The application of anatomical constraints resulted not only in reliable measurements of the architecture of human calf muscles, but also in measurements that were insensitive to variations in tractography parameters.

The reliability of the measurements presented here is higher than the reliability reported in previous studies that used DTI tractography to measure muscle architecture in humans. Sinha and Sinha (2011) reported coefficient of variations of 6–10% in the medial gastrocnemius muscle. Their analysis was limited to selected locations within the muscle, because at other locations fibre tracking gave implausible results. Heemskerk et al. (2010) reported moderate repeatability of fascicle length measurements in the tibialis anterior muscle. They also used quantitative criteria to select plausible fibres from all fibres generated by DTI tractography (Heemskerk et al., 2009), but these criteria did not use information from anatomical scans to constrain fascicle origins and insertions to anatomically realistic locations.

To our knowledge, no previous studies have systematically evaluated the sensitivity of muscle architecture measurements to

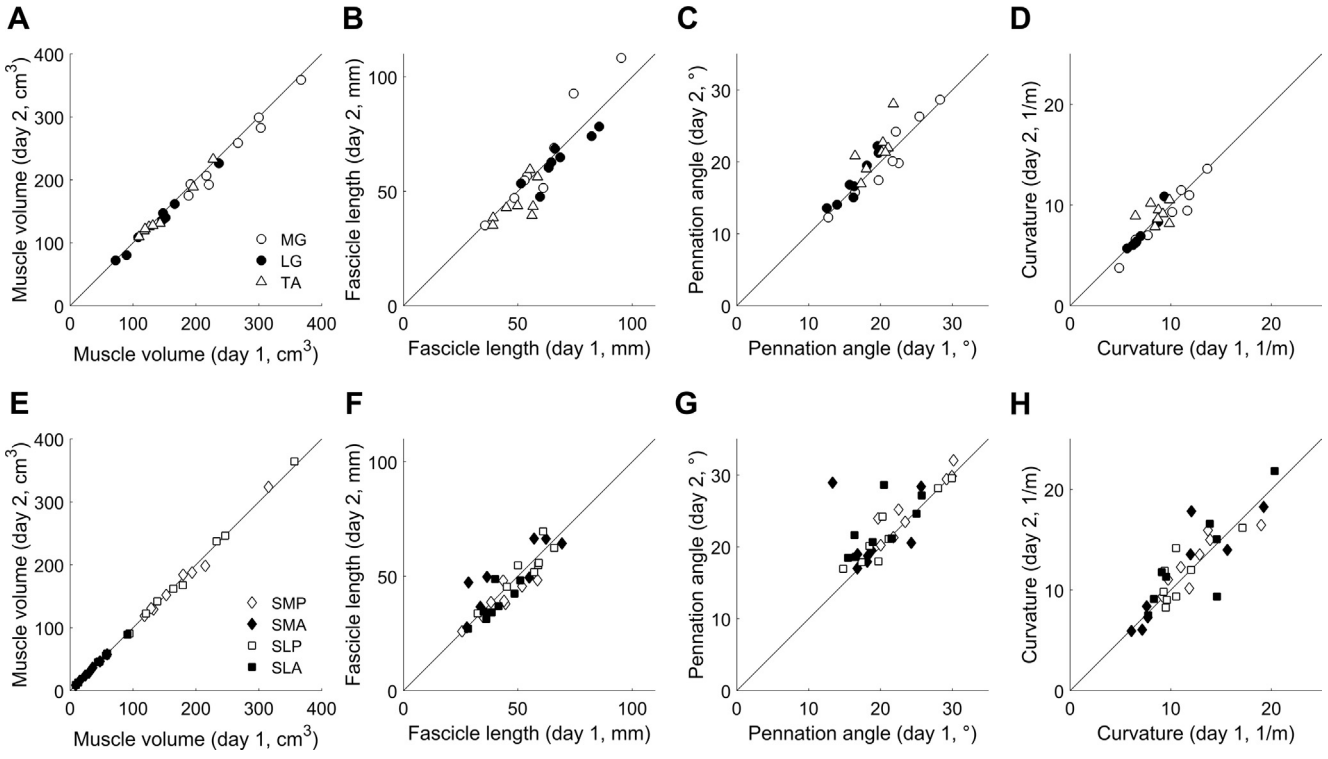

Fig. 2. Relationship between measurements obtained on day 1 and day 2 for muscle volume (A, E), fascicle length (B, F), pennation angle (C, G) and curvature (D, H). The top row presents data for the medial gastrocnemius (MG), lateral gastrocnemius (LG) and tibialis anterior (TA) and the bottom row presents data for the soleus, which was separated in four compartments (SMP: medial-posterior, SMA: medial-anterior, SLP: lateral-posterior, SLA: lateral-anterior).

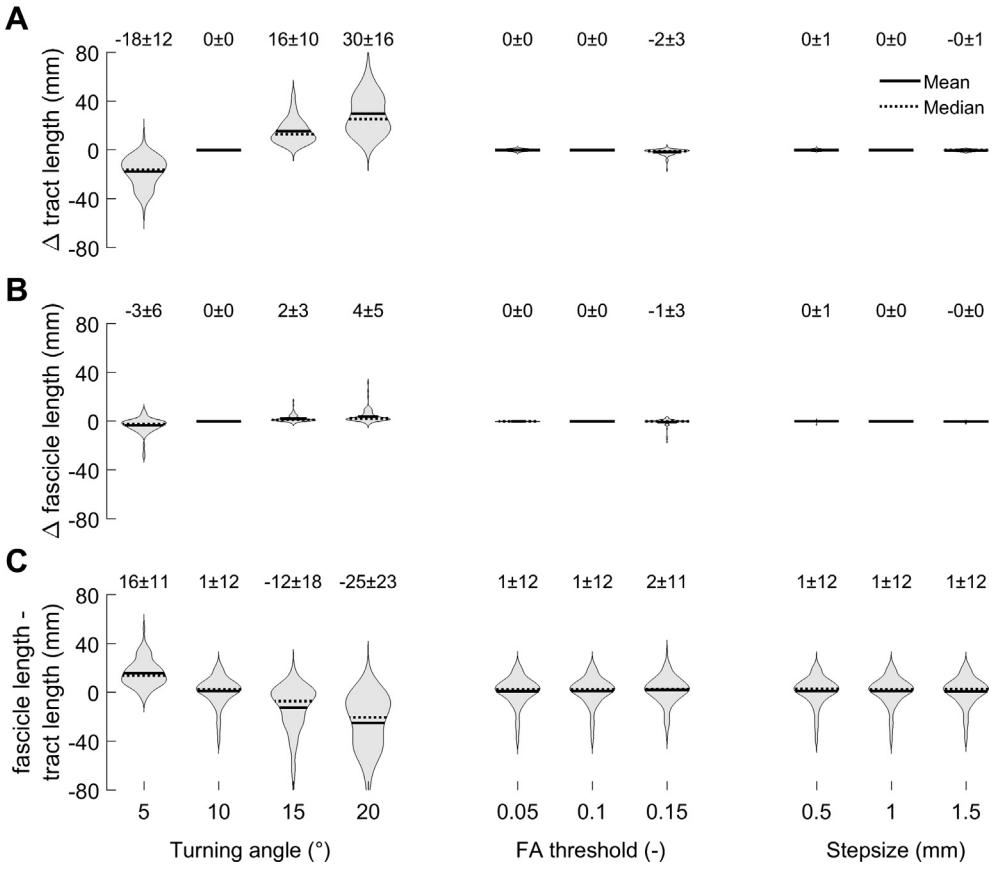

Fig. 3. Effect of tractography settings on tract lengths (A), fascicle lengths (B), and the difference between fascicle lengths and tract lengths (C). (A and B) Violin plots show distributions of the difference in tract lengths and fascicle lengths obtained by systematically varying, one at a time, the maximum turning angle, fractional anisotropy (FA) threshold or stepsize. The difference values indicate the lengths obtained with the parameter variation minus the lengths obtained with the default settings (turning angle = 10°, FA threshold = 0.1, step size = 1 mm). (C) Distributions of the difference between fascicle lengths and tract lengths for all tractography settings. Each group contains 112 values (seven muscles or muscle compartments of eight participants, each of whom was measured twice). The violin plot widths illustrate kernel probability density, i.e. the width of the shaded area represents the proportion of the data located there. Values above each violin plot indicate the mean ± standard deviation of the distribution.

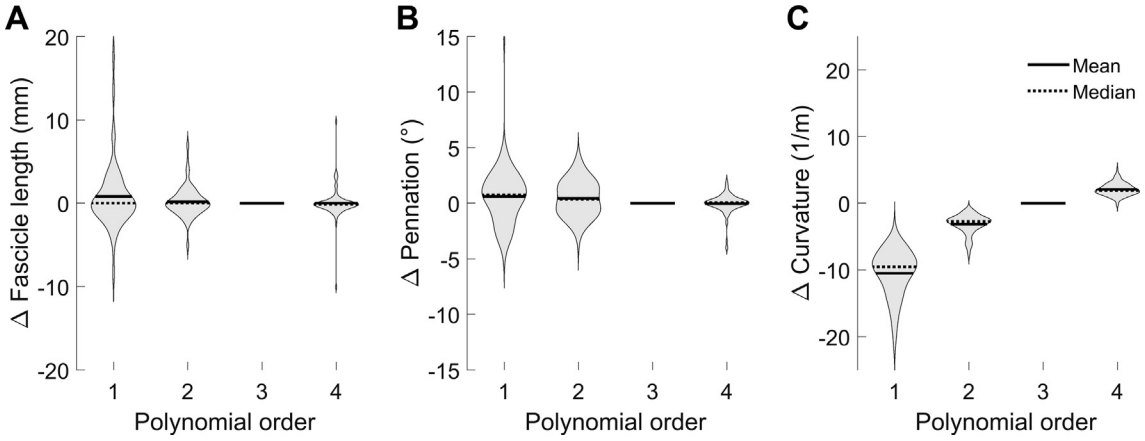

Fig. 4. Effect of polynomial order on muscle architecture measurements. Violin plots illustrate fascicle length (A), pennation angle (B) and curvature (C) obtained with polynomials of order 1, 2, 3 and 4 minus those values obtained with the default polynomial order of 3. Each group contains 112 values (7 muscle compartments of 8 participants, which each were measured twice). The violin plot widths illustrate kernel probability density, i.e. the width of the shaded area represents the proportion of the data located there.

tractography stopping criteria. The sensitivity analysis presented here shows that fibre tract lengths were influenced much more by the choice of maximum turning angle than by the choice of step size or minimum FA threshold (Fig. 3). The sensitivity of fibre tract lengths to variations in turning angle is a major limitation of conventional DTI tractography techniques because it is unknown which angle leads to the most accurate measurements. Moreover, it is likely that variations in muscle architecture between muscles and differences in noise levels between scans require that different stopping criteria are applied in different settings. When anatomical

constraints were applied to fibre tracts, the sensitivity to variations in the turning angle was reduced significantly. Varying the turning angle from 10° to 20° changed fibre tract lengths by, on average, 30 mm, but changed fascicle lengths by only 4 mm. The more robust measurement of fascicle lengths than tract lengths suggests that anatomical constraints should be applied to obtain anatomically realistic measurements of muscle architecture from DTI data.

To reconstruct fascicles, polynomial curves were fitted to fibre tracts, but it is not clear which order of polynomial provided the most accurate muscle architecture measurements. Damon et al. (2012) fitted polynomial curves to fibre tracts and concluded, based on simulations, that second order curves provided accurate measurements of curvature and pennation angle. We varied the polynomial order between 1 and 4 and found only small mean absolute differences in fascicle lengths and pennation angles of 1–3 mm and 0.5–2°, respectively (Fig. 4). While polynomial order only had a minor effect on fascicle lengths and pennation angle, curvature was influenced significantly by the order. As expected, higher orders provided larger curvatures. Based on current data it is not possible to determine which order provided the most accurate measurements. However, we recommend the use of third order polynomials as we have done previously (Bolsterlee et al., 2017; Bolsterlee et al., 2018), to leave open the possibility that fascicles are S-shaped. Although curvature was measured with high reliability in all muscles except the TA, the effect of polynomial order on curvature should be kept in mind when interpreting fascicle curvatures. Future studies could use detailed *ex vivo* measurements of muscle architecture from quantitative microdissection (Lee et al., 2015) or microCT (Kupczik et al., 2015) to determine the polynomial order that provides the most accurate measurements of fascicle curvatures.

To date, only deterministic tractography algorithms have been applied successfully to quantify muscle architecture in human skeletal muscle, but probabilistic tractography algorithms, which have been applied successfully to reconstruct white matter tracts in the brain, may prove useful as well. One popular probabilistic method uses fibre orientation distribution functions (Tournier et al., 2004) to correctly reconstruct the complex fibre structure of white matter tracts in the brain when multiple fibre directions are present within one voxel (fibre crossing). The added value of more complex and computationally expensive approaches to fibre tracking may be limited in muscle tissue, as fibre orientations in skeletal muscle are more homogeneous than the orientations of white matter tracts in the brain (e.g. muscle fibres do not cross). Nevertheless, probabilistic tractography methods, or methods that fit constrained fibre fields on diffusion tensor imaging data of human skeletal muscle (Levin et al., 2011) are likely to perform better in the presence of noise, and may thus provide more accurate measurements of muscle architecture.

The current study does not provide evidence for the validity of the DTI-based measurements of muscle architecture. Ideally, the validity needs to be demonstrated on human muscles using the same clinical scanners and protocols as used *in vivo,* as this would constitute stronger evidence than provided by previous studies which used tissue-mimicking phantoms (Berry et al., 2017) or compared direct measurements of the architecture of animal muscles to DTI-based measurements using high field-strength animal scanners (4.7 Tesla; Damon et al., 2002) or scan times infeasible for human studies (69 min; Schenk et al., 2013). We have attempted to compare DTI-based measurements from human cadaver muscles to direct measurements using microdissection (unpublished data). However, using similar imaging protocols as used in the present study, we were not able to reconstruct the architecture from the muscles of fresh-frozen cadavers, which were thawed before scanning, at the same high quality as from human muscles *in vivo*. We hypothesized that the microstructure of the muscle tissue, which determines the diffusion properties and thus the quality of the reconstructions, was disrupted by freezing and thawing. Despite these limitations in determining the accuracy of DTI-based measurements of the architecture of human skeletal muscle, we believe our measurements to be reasonably accurate. Our microdissection studies on several human muscles suggest there is very little change in fibre orientation close to the aponeuroses, so the small linear extrapolations of the fascicles near the aponeuroses (on average 11% of fascicle length; Table 2) are unlikely to bias the measurements significantly, at least not in relaxed muscles. An additional reason to trust the validity of our measurements is that we have previously shown that the mean fascicle lengths obtained with our approach are very similar to those obtained using ultrasonography (Bolsterlee et al., 2015) and cadaver dissection (Ward et al., 2009). Moreover, we have measured realistic amounts of lengthening in fascicles of the medial gastrocnemius (Bolsterlee et al., 2017) and soleus (Bolsterlee et al., 2018) during passive ankle rotation.

Experimental data and simulations have demonstrated the important role of 3D deformation to generation of muscle force in actively contracting muscle, and this has generated an interest in the 3D structure of human muscles (Azizi et al., 2017; Böl et al., 2013). In the last decade, a number of methods other than DTI have been developed to measure 3D muscle architecture in humans *in vivo*. For example, 3D ultrasound, in which multiple 2D ultrasound images are stitched together to form a 3D image of the muscle, can be used to measure muscle volumes and, at selected locations in the muscle, fascicle lengths and pennation angles (Barber et al., 2009; van der Zwaard et al., 2018). The 3D architecture of muscles can also be reconstructed using a computational fluid dynamics (CFD) approach, which assumes that fascicles are aligned with the direction of a hypothetical fluid flowing from the aponeurosis of origin to the insertion of the muscle (Choi and Blemker, 2013). The CFD method is especially promising for simulation studies, in which continuous measurements of fibre orientations are required to study 3D contraction mechanisms. In contrast, ultrasound and DTI will presumably prove more useful than CFD methods in experimental studies seeking to reveal mechanisms of 3D muscle architecture with, for instance, training, growth, ageing or disease. Given the limitations and inaccuracies of all currently available methods for measuring muscle architecture in 3D, converging evidence from different methods would constitute the strongest evidence of architectural adaptations in muscles.

Acknowledgements

The study was supported by the Australian National Health and Medical Research Council (NHMRC; Program Grant APP1055084). R. Herbert is supported by a research fellowship from the Australian NHMRC. A. D'Souza is supported by a Royal Freemasons' Benevolence Institution Scholarship.

Conflict of interest statement

I hereby state that neither I, nor any of the other authors, have had any financial or personal relationships with other people or organisations that could inappropriately influence (bias) our work.

References

Agur, A.M., Ng-Thow-Hing, V., Ball, K.A., Fiume, E., McKee, N.H., 2003. Documentation and three-dimensional modelling of human soleus muscle architecture. Clin. Anat. 16 (4), 285–293.

Andersson, J.L.R., Sotiropoulos, S.N., 2016. An integrated approach to correction for off-resonance effects and subject movement in diffusion MR imaging. Neuroimage 125, 1063–1078.

Azizi, E., Brainerd, E.L., Roberts, T.J., 2008. Variable gearing in pennate muscles. Proc. Natl. Acad. Sci. 105 (5), 1745–1750.
Azizi, E., Deslauriers, A.R., Holt, N.C., Eaton, C.E., 2017. Resistance to radial expansion limits muscle strain and work. Biomech. Model Mechanobiol. 16 (5), 1633–1643.
Barber, L., Barrett, R., Lichtwark, G., 2009. Validation of a freehand 3D ultrasound system for morphological measures of the medial gastrocnemius muscle. J. Biomech. 42 (9), 1313–1319.
Basser, P.J., Mattiello, J., LeBihan, D., 1994. MR diffusion tensor spectroscopy and imaging. Biophys. J. 66 (1), 259–267.
Basser, P.J., Pierpaoli, C., 1996. Microstructural and physiological features of tissues elucidated by quantitative-diffusion-tensor MRI. J. Magn. Reson., Ser. B 111 (3), 209–219.
Berry, D.B., You, S.T., Warner, J., Frank, L.R., Chen, S.C., Ward, S.R., 2017. A 3D tissue-printing approach for validation of diffusion tensor imaging in skeletal muscle. Tissue Eng. Part A 23 (17–18), 980–988.
Blemker, S.S., Pinsky, P.M., Delp, S.L., 2005. A 3D model of muscle reveals the causes of nonuniform strains in the biceps brachii. J. Biomech. 38 (4), 657–665.
Böl, M., Leichsenring, K., Weichert, C., Sturmat, M., Schenk, P., Blickhan, R., Siebert, T., 2013. Three-dimensional surface geometries of the rabbit soleus muscle during contraction: input for biomechanical modelling and its validation. Biomech. Model. Mechanobiol. 12 (6), 1205–1220.
Bolsterlee, B., D'Souza, A., Gandevia, S.C., Herbert, R.D., 2017. How does passive lengthening change the architecture of the human medial gastrocnemius muscle? J. Appl. Physiol. 122 (4), 727–738.
Bolsterlee, B., Finni, T., D'Souza, A., Eguchi, J., Clarke, E.C., Herbert, R.D., 2018. Three-dimensional architecture of the whole human soleus muscle in vivo. PeerJ 6, e4610.
Bolsterlee, B., Veeger, H.E.J., van der Helm, F.C.T., Gandevia, S.C., Herbert, R.D., 2015. Comparison of measurements of medial gastrocnemius architectural parameters from ultrasound and diffusion tensor images. J. Biomech. 48 (6), 1133–1140.
Burakiewicz, J., Hooijmans, M.T., Webb, A.G., Verschuuren, J.J.G.M., Niks, E.H., Kan, H.E., 2018. Improved olefinic fat suppression in skeletal muscle DTI using a magnitude-based dixon method. Magn. Reson. Med. 79 (1), 152–159.
Choi, H.F., Blemker, S.S., 2013. Skeletal muscle fascicle arrangements can be reconstructed using a laplacian vector field simulation. PLoS ONE 8 (10), e77576.
Cronin, N.J., Lichtwark, G., 2013. The use of ultrasound to study muscle-tendon function in human posture and locomotion. Gait & Posture 37 (3), 305–312.
Damon, B.M., Ding, Z.H., Anderson, A.W., Freyer, A.S., Gore, J.C., 2002. Validation of diffusion tensor MRI-based muscle fiber tracking. Magn. Reson. Med. 48 (1), 97–104.
Damon, B.M., Froeling, M., Buck, A.K., Oudeman, J., Ding, Z., Nederveen, A.J., Bush, E. C., Strijkers, G.J., 2017. Skeletal muscle diffusion tensor-MRI fiber tracking: rationale, data acquisition and analysis methods, applications and future directions. NMR Biomed. 30 (3).
Damon, B.M., Heemskerk, A.M., Ding, Z.H., 2012. Polynomial fitting of DT-MRI fiber tracts allows accurate estimation of muscle architectural parameters. Magn. Reson. Imaging 30 (5), 589–600.
Fang, Q.Q., Boas, D.A., 2009. Tetrahedral mesh generation from volumetric binary and gray-scale images. In: Proceedings of IEEE International Symposium on Biomedical Imaging, pp. 1142–1145.
Fedorov, A., Beichel, R., Kalpathy-Cramer, J., Finet, J., Fillion-Robin, J.-C., Pujol, S., Bauer, C., Jennings, D., Fennessy, F., Sonka, M., 2012. 3D Slicer as an image computing platform for the Quantitative Imaging Network. Magn. Reson. Imaging 30 (9), 1323–1341.
Froeling, M., Nederveen, A.J., Heijtel, D.F.R., Lataster, A., Bos, C., Nicolay, K., Maas, M., Drost, M.R., Strijkers, G.J., 2012. Diffusion-tensor MRI reveals the complex muscle architecture of the human forearm. J. Magn. Reson. Imaging 36 (1), 237–248.
Froeling, M., Nederveen, A.J., Nicolay, K., Strijkers, G.J., 2013. DTI of human skeletal muscle: the effects of diffusion encoding parameters, signal-to-noise ratio and T2 on tensor indices and fiber tracts. NMR Biomed. 26 (11), 1339–1352.
Fukunaga, T., Ichinose, Y., Ito, M., Kawakami, Y., Fukashiro, S., 1997. Determination of fascicle length and pennation in a contracting human muscle in vivo. J. Appl. Physiol. 82 (1), 354–358.
Heemskerk, A.M., Sinha, T.K., Wilson, K.J., Ding, Z.H., Damon, B.M., 2009. Quantitative assessment of DTI-based muscle fiber tracking and optimal tracking parameters. Magn. Reson. Med. 61 (2), 467–472.
Heemskerk, A.M., Sinha, T.K., Wilson, K.J., Ding, Z.H., Damon, B.M., 2010. Repeatability of DTI-based skeletal muscle fiber tracking. NMR Biomed. 23 (3), 294–303.
Herbert, R.D., Heroux, M.E., Diong, J., Bilston, L.E., Gandevia, S.C., Lichtwark, G.A., 2015. Changes in the length and three-dimensional orientation of muscle fascicles and aponeuroses with passive length changes in human gastrocnemius muscles. J. Physiol. 593 (2), 441–455.
Klein, S., Staring, M., Murphy, K., Viergever, M.A., Pluim, J.P., 2010. elastix: a toolbox for intensity-based medical image registration. IEEE Trans. Med. Imaging 29 (1), 196–205.
Kupczik, K., Stark, H., Mundry, R., Neininger, F.T., Heidlauf, T., Röhrle, O., 2015. Reconstruction of muscle fascicle architecture from iodine-enhanced microCT images: a combined texture mapping and streamline approach. J. Theor. Biol. 382, 34–43.
Lee, D., Li, Z., Sohail, Q.Z., Jackson, K., Fiume, E., Agur, A., 2015. A three-dimensional approach to pennation angle estimation for human skeletal muscle. Comput. Methods Biomech. Biomed. Eng. 18 (13), 1474–1484.
Levin, D.I.W., Gilles, B., Madler, B., Pai, D.K., 2011. Extracting skeletal muscle fiber fields from noisy diffusion tensor data. Med. Image Anal. 15 (3), 340–353.
Manjon, J.V., Coupe, P., Concha, L., Buades, A., Collins, D.L., Robles, M., 2013. Diffusion weighted image denoising using overcomplete local PCA. PLoS ONE 8 (9), e73021.
McGraw, K.O., Wong, S.P., 1996. Forming inferences about some intraclass correlation coefficients. Psychol. Methods 1 (1), 30–46.
Oudeman, J., Nederveen, A.J., Strijkers, G.J., Maas, M., Luijten, P.R., Froeling, M., 2015. Techniques and applications of skeletal muscle diffusion tensor imaging: a review. J. Magn. Reson. Imaging, 773–788.
Raiteri, B.J., Cresswell, A.G., Lichtwark, G.A., 2018. Muscle-tendon length and force affect human tibialis anterior central aponeurosis stiffness in vivo. Proc. Natl. Acad. Sci. 115 (14), E3097–E3105.
Ross, S.A., Ryan, D.S., Dominguez, S., Nigam, N., Wakeling, J.M., 2018. Size, history-dependent, activation and three-dimensional effects on the work and power produced during cyclic muscle contractions. Integr. Comp. Biol. 58 (2), 232–250.
Schenk, P., Siebert, T., Hiepe, P., Gullmar, D., Reichenbach, J.R., Wick, C., Blickhan, R., Bol, M., 2013. Determination of three-dimensional muscle architectures: validation of the DTI-based fiber tractography method by manual digitization. J. Anat. 223 (1), 61–68.
Sinha, S., Sinha, U., 2011. Reproducibility analysis of diffusion tensor indices and fiber architecture of human calf muscles in vivo at 1.5 Tesla in neutral and plantarflexed ankle positions at rest. J. Magn. Reson. Imaging 34 (1), 107–119.
Tournier, J.D., Calamante, F., Gadian, D.G., Connelly, A., 2004. Direct estimation of the fiber orientation density function from diffusion-weighted MRI data using spherical deconvolution. Neuroimage 23 (3), 1176–1185.
van der Zwaard, S., Weide, G., Levels, K., Eikelboom, M.R.I., Noordhof, D.A., Hofmijster, M.J., van der Laarse, W.J., de Koning, J.J., de Ruiter, C.J., Jaspers, R. T., 2018. Muscle morphology of the vastus lateralis is strongly related to ergometer performance, sprint capacity and endurance capacity in Olympic rowers. J. Sports Sci. 36 (18), 2111–2120.
Ward, S.R., Eng, C.M., Smallwood, L.H., Lieber, R.L., 2009. Are current measurements of lower extremity muscle architecture accurate? Clin. Orthop. Relat. Res. 467 (4), 1074–1082.
Yeh, F.C., Verstynen, T.D., Wang, Y.B., Fernandez-Miranda, J.C., Tseng, W.Y.I., 2013. Deterministic diffusion fiber tracking improved by quantitative anisotropy. PLoS ONE 8 (11), e80713.
Yushkevich, P.A., Piven, J., Hazlett, H.C., Smith, R.G., Ho, S., Gee, J.C., Gerig, G., 2006. User-guided 3D active contour segmentation of anatomical structures: Significantly improved efficiency and reliability. Neuroimage 31 (3), 1116–1128.